The Astrophysical Journal, 659:541–548, 2007 April 10

MODELING THE HARD STATES OF XTE J1550−564 DURING ITS 2000 OUTBURST

Feng Yuan,[1,2,3] Andrzej A. Zdziarski,[4] Yongquan Xue,[2] and Xue-Bing Wu[5]

Received 2006 August 22; accepted 2006 December 23

ABSTRACT

We study the hard states of the black hole binary XTE J1550−564 during its 2000 outburst. In order to explain those states at their highest luminosities, $L \sim 10\%$ of the Eddington luminosity, $L_{\rm E}$, we propose a specific hot accretion flow model. We point out that the highest values of the hard-state L are substantially above the L that an advection-dominated accretion flow can produce, $\sim 0.4\alpha^2 L_{\rm E}$, which is only $\sim$3%–4% of $L_{\rm E}$ even for α as high as 0.3. On the other hand, we successfully explain the hard states with $L \sim 0.04$–0.10 using the luminous hot accretion flow (LHAF) model. As $0.10L_{\rm E}$ is also roughly the highest luminosity an LHAF can produce, such agreement between the predicted and observed highest luminosities itself provides strong support for this model. We then study multiwaveband spectral variability during the 2000 outburst. In addition to the primary maxima in the optical light curves, secondary maxima were detected after the transition from the very high state to the hard state. We show that the secondary maxima are well modeled as synchrotron emission from a jet formed during the state transition. We argue that the absence of a corresponding secondary peak in the X-ray light curve indicates that the X-ray jet emission, regardless of its radiative process, synchrotron or Comptonization, is not important in the hard state as compared with the emission from the accretion flow.

Subject headings: accretion, accretion disks — black hole physics — ISM: jets and outflows — stars: individual (XTE J1550−564) — X-rays: stars

1. INTRODUCTION

Black hole X-ray binaries (BHXBs) appear in five main spectral states, namely, quiescent, low/hard, intermediate, high/soft, and very high (see, e.g., McClintock & Remillard 2006 [although they prefer a different nomenclature]). The origin of the X-ray spectrum of the hard state represents a highly interesting problem. The presence of a universal high-energy spectral cutoff above $\sim$100–200 keV in the hard state points to the X-ray emission's coming from thermal Comptonization in a hot accretion corona with an electron temperature of $\sim 10^9$ K $\simeq (10^2$ keV$)/k$ (for reviews, see, e.g., Zdziarski 2000; Zdziarski & Gierliński 2004). We note that an alternative jet model (Markoff et al. 2005), although also relying on thermal Comptonization as the dominant component at photon energies $\gtrsim$10 keV, requires that the electron temperature be 30–40 times higher, $kT \sim 3$–4 MeV. Then the origin of the $\sim$100 keV cutoff is not clear; if it is due to the first-order scattering by those thermal electrons, very careful fine-tuning is required in order to achieve the observed cutoff energy. On the other hand, higher order scatterings will yield another spectral cutoff at $\gtrsim 3kT \sim 10$ MeV, the presence of which remains to be observationally tested.

There are two different main models of the hot corona. One relies on electron heating by magnetic reconnection above a standard thin disk (Liang & Price 1977; Galeev et al. 1979). Since the process of magnetic reconnection remains poorly understood, this model has not yet been elaborated upon in detail, although recent numerical simulations have shed some light on the problem (Hirose et al. 2006). The other model is a hot accretion flow, which is advection dominated (ADAF) in most of its parameter space (Rees et al. 1982; Narayan & Yi 1994, 1995; Abramowicz et al. 1995). We need to highlight two points when we use the term ADAF. First, it is known that in most of the ADAF parameter space, outflow is moderately strong, as emphasized by Blandford & Begelman (1999; the adiabatic inflow-outflow solution) and other authors. Second, as we show below, another hot accretion solution may be responsible for the X-ray emission of the relatively luminous hard states. Compared with magnetic reconnection, an ADAF has clear dynamics, and its astrophysical applications can be worked out in detail. The specific suggestion of applying the ADAF to the hard state is due to Narayan (1996) and Narayan et al. (1996; see also Shapiro et al. 1976 [who, however, did not recognize the importance of advection]). The first detailed comparisons of calculations with data were then done by Esin et al. (1997, hereafter E97).

In the present paper, we concentrate on hot accretion flows. We note that the radiative efficiency of an ADAF increases with the accretion rate, $\dot{M}$. Thus, an ADAF can explain not only very dim sources such as the Galactic center (e.g., Yuan et al. 2003), but also some relatively luminous sources such as hard-state BHXBs. The highest rate, called the critical accretion rate, of an ADAF is determined by the balance between viscous heating and cooling, $q_{\rm vis} \approx q_{\rm ie}$, which occurs at $\dot{M}_{\rm ADAF} \sim 10\alpha^2 \dot{M}_{\rm E}$, where α is the viscosity parameter, $\dot{M}_{\rm E} \equiv L_{\rm E}/c^2$, q is the rate of energy change per unit volume, and $L_{\rm E}$ is the Eddington luminosity. The corresponding maximum luminosity is $L_{\rm ADAF} \sim 0.4\alpha^2 L_{\rm E}$ (E97).[6] The actual value of α remains uncertain, but recent three-dimensional magnetohydrodynamic (MHD) numerical simulations suggest $\alpha \sim 10^{-2}$ to 10^{-1} in most of the disk midplane (Hawley & Krolik 2001). Even for α as high as 0.3 (a commonly used value in ADAF studies), the maximum ADAF luminosity is still only $\simeq (0.03$–$0.04) L_{\rm E}$. It has been thought that above $L_{\rm ADAF}$, there is no hot accretion solution, with a thin disk remaining the only viable solution.

However, observations of the hard state in BHXBs often show higher luminosities during the rising part of an outburst. For example, the hard state of XTE J1550−564 reached $0.20L_{\rm E}$ (Sobczak et al. 2000) and $\sim 0.10L_{\rm E}$ (Rodriguez et al. 2003; this work) during

[1] Shanghai Astronomical Observatory, Chinese Academy of Sciences, 200030 Shanghai, China; fyuan@shao.ac.cn.
[2] Department of Physics, Purdue University, West Lafayette, IN 47907.
[3] Joint Institute for Galaxy and Cosmology (JOINGC) of Shanghai Astronomical Observatory and the University of Science and Technology of China.
[4] Centrum Astronomiczne im. Mikołaja Kopernika, 00-716 Warsaw, Poland.
[5] Department of Astronomy, Peking University, 100871 Beijing, China.

[6] Thus, the highest radiative efficiency of an ADAF is $\simeq$0.04, not much lower than that of a standard thin disk around a Schwarzschild black hole ($\simeq$0.057).

its outbursts in 1998 and 2000, respectively. The highest hard-state luminosity of GX 339−4 was $\simeq(0.25-0.30)L_{\rm E}$ (Zdziarski et al. 2004; Done & Gierliński 2003). These observational results have long presented a puzzle for the hot accretion flow models.

Of importance in this context is the finding of a new hot accretion flow solution, the so-called luminous hot accretion flow (LHAF; Yuan 2001, hereafter Y01). Different from an ADAF, this solution corresponds to accretion rates above the ADAF critical rate, $\dot{M}_{\rm ADAF}$, up to another critical accretion rate that is about 3−5 times higher for the parameters adopted in Y01. In addition to the accretion rate, the radiative efficiency of an LHAF is also higher than that of a typical ADAF. Therefore, an LHAF can produce much higher luminosity than an ADAF. Yuan & Zdziarski (2004) studied some luminous hard states of BHXBs and active galactic nuclei and found that their relatively low electron temperatures and high luminosities do require an LHAF to be present. In the first part of this work, we apply this approach to hard-state spectra of XTE J1550−564 during its 2000 outburst.

In addition to studying X-ray spectra alone, more and more efforts are being devoted to multiwavelength, simultaneous observations and modeling of BHXBs, as illustrated, for example, by studies of XTE J1118+480. Nearly simultaneous observations of this source have been conducted from radio to X-ray wavelengths (e.g., Hynes et al. 2000; McClintock et al. 2001; Frontera et al. 2001, 2003; Chaty et al. 2003). These have allowed important theoretical conclusions to be drawn. Esin et al. (2001) showed that the extreme-ultraviolet (EUV) data rule out models with a thin disk extending to the last stable orbit. Using a coupled jet-ADAF model, Yuan et al. (2005) and Malzac et al. (2004) successfully explained the radio–to–X-ray spectrum and most of the timing properties of the source.

Here we apply the same approach to XTE J1550−564. We use simultaneous multiwavelength observations at radio, infrared, optical, and X-ray wavelengths during the 2000 outburst (Corbel et al. 2001; Jain et al. 2001, hereafter J01; Tomsick et al. 2001; Rodriguez et al. 2003). Compared with XTE J1118+480, XTE J1550−564 is much more luminous. During the outburst, transitions between the hard and very high states occurred, unlike the case of XTE J1118+480, which was always in the hard state. Therefore, some interesting new phenomena were observed. One issue we discuss below is that of secondary maxima in the IR/optical light curves. J01 reported infrared (H), optical (I, V), and X-ray light curves for the 2000 outburst. After reaching the peak of the outburst, the fluxes declined in all of these bands, and a transition from the very high state to the hard state occurred around MJD 51,680. Afterward, the X-ray flux continued to decline, whereas the IR/optical light curves began to rise and reached secondary maxima at MJD 51,699–51,705; after that, they declined again. A contemporaneous spectrum in the radio band was obtained by Corbel et al. (2001) at MJD 51,697. Here we model the simultaneous radio, IR, optical, and X-ray data and explain the secondary IR/optical maxima.

In § 2, we model the X-ray emission of the hard states, paying special attention to the dynamics of the hot accretion flow. In § 3, we study the simultaneous radio, IR/optical, and X-ray data during the decline phase and explain the secondary IR/optical maxima. We conclude in § 4 with a summary and discussion.

2. MODELING THE X-RAY SPECTRA OF THE HARD STATES OF XTE J1550−564

2.1. *Observational Data*

During its 2000 outburst, XTE J1550−564 experienced hard and very high states. We have selected four occurrences of the hard state, at MJD 51,646, 51,658, 51,687, and 51,696, based on the criteria that they span a wide range of X-ray luminosity and that each includes simultaneous optical data. Their spectra are shown in Figure 1 in different colors. For comparison, we also show an example of the very high state spectrum, from MJD 51,662. These *Rossi X-Ray Timing Explorer* (*RXTE*) spectra were earlier studied by Rodriguez et al. (2003) and Tomsick et al. (2001); here we have reextracted them ourselves. They can be well fitted by a power-law form with an exponential cutoff. The X-ray spectra in blue, red, green, and magenta in Figure 1 (*top to bottom*) are fitted with a photon index and e-folding energy, (Γ, E_f), of $(1.70 \pm 0.01,\ 115 \pm 5.6)$, $(1.46 \pm 0.01,\ 137^{+8}_{-7})$, $(1.53 \pm 0.01,\ 200^{+80}_{-50})$, and $(1.53 \pm 0.01,\ 460^{+340}_{-240})$, respectively. We see a strong anticorrelation between the X-ray flux and E_f, the value of which monotonically increases with decreasing flux.

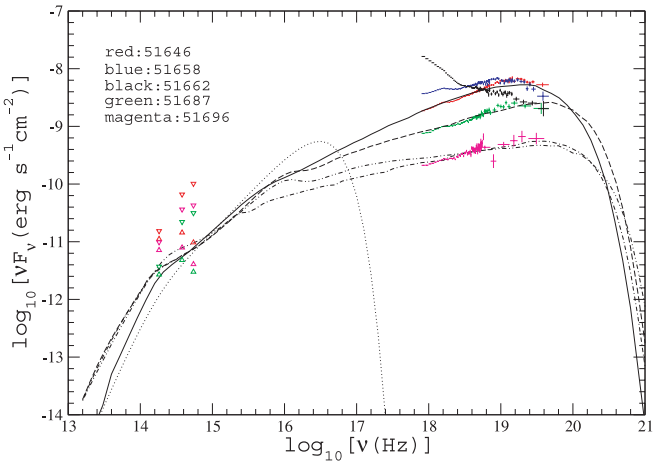

FIG. 1.—Spectral fitting results for the hard states of XTE J1550−564 during its 2000 outburst at different dates. The two sets of optical data for each date correspond to the two limiting values of the extinction, $A_V = 4.75$ and $A_V = 2.2$. The parameters of the hot accretion flow models are $\dot{M}_0 = 1.0\dot{M}_{\rm E}$ and $s_0 = 0.55$ (*dot-dashed curve*), $\dot{M}_0 = 1.1\dot{M}_{\rm E}$ and $s_0 = 0.3$ (*dashed curve*), and $\dot{M}_0 = 1.3\dot{M}_{\rm E}$ and $s_0 = 0.3$ (*solid curve*). The dot-dashed curve shows an ADAF model, while the other two models are LHAFs (see Fig. 2). The double-dot–dashed curve shows a model without an outflow, to illustrate its hardening effect on the X-ray slope (see § 2.3). The dotted curve shows the emission from a truncated thin disk at $\dot{M} = 1.3\dot{M}_{\rm E}$ and $r_{\rm tr} = 100r_{\rm S}$. We see that the inclusion of this component improves the fit in the optical range, but it is not sufficient to explain the IR data.

The IR/optical data in Figure 1 are from J01. Since we do not know the exact value of the extinction, we show two sets of fluxes for each spectrum, corresponding to the two extinction limits $A_V = 4.75$ (Orosz et al. 2002) and $A_V = 2.2$ (Sánchez-Fernández et al. 1999). The details of the data reduction can be found in Xue et al. (2006).

2.2. *Accretion Flow Models*

We now fit the spectra using our accretion flow model. Its components are nearly the same as in E97, that is, the model consists of an inner hot accretion flow (ADAF or LHAF) within a transition radius, $r_{\rm tr}$, and an outer thin disk. We assume that only a fraction of the accretion rate at $r_{\rm tr}$ actually accretes onto the black hole; the rest is ejected. This assumption is required both by numerical simulations (Stone et al. 1999; Hawley & Balbus 2002; Igumenshchev et al. 2003) and by analytical work (Narayan & Yi 1994; Blandford & Begelman 1999; Narayan et al. 2000; Quataert & Gruzinov 2000). Details of this process depend on the accretion rate. Here, in order to formally take into account the role of outflows as well as convection in modifying the density

profile of the accretion flow, we assume, following Yuan et al. (2005), that $\dot{M}(r) = \dot{M}_0$ for $r \geq r_{\rm tr}$ and

$$\frac{d \ln \dot{M}(r)}{d \ln r} = s(r) \quad \text{for } r < r_{\rm tr}, \tag{1}$$

where

$$s(r) = s_0 \max\left[f(r), 0\right] \tag{2}$$

and s_0 is independent of r but can be different for different values of $\dot{M}_0$. The above formula is based on the consideration that the outflow (and convection) is ultimately due to the acquisition of a positive Bernoulli parameter by the accreting gas, as emphasized by Narayan & Yi (1994), which value is smaller for higher accretion rates because of the stronger radiative energy loss. Then $f(r)$ is the advection factor of the accretion flow, defined as

$$f(r) \equiv \frac{q_{\rm adv}}{q_{\rm vis}} = \frac{q_{\rm vis} - q_{\rm ie}}{q_{\rm vis}}. \tag{3}$$

A negative value of f implies that advection plays a heating rather than a cooling role. In this case, the hot accretion flow is in the LHAF regime (Y01), as we point out in § 2.3. When $\dot{M}$ is very low, $f(r) = 1$ and $s(r) = s_0$. In this case, equation (1) gives us the usual form, $\dot{M} = \dot{M}_0(r/r_{\rm tr})^{s_0}$ (e.g., Blandford & Begelman 1999).

We calculate global solutions for the hot accretion flow using the method of Y01. A major difference of this method with respect to that of E97 is that we solve the radiation hydrodynamics equations self-consistently and thus obtain $f(r)$ at each radius. In contrast, E97 used the approximation of $f(r)$ having a constant average value at all radii. The radiation processes we consider include bremsstrahlung, synchrotron emission, and Comptonization of both synchrotron photons from the hot accretion flow and soft photons from the thin disk. We use formulae from Narayan & Yi (1995) and Coppi & Blandford (1990) to calculate the synchrotron and Comptonization spectra, respectively, as functions of the radius. We treat self-absorption as in Manmoto et al. (1997). The emission from the outer, cool disk is modeled as a multicolor blackbody spectrum. The temperature as a function of r is determined by the viscous dissipation and the irradiation of the disk by the inner hot flow. E97 show that when $r_{\rm tr} \gtrsim 30 r_{\rm S}$, the outer thin disk has little effect on the X-ray emission from the inner, hot accretion flow because the seed photons for Comptonization mainly come from the synchrotron and bremsstrahlung emissions in the hot accretion flow. (Here $r_{\rm S} \equiv 2GM/c^2$ is the Schwarzschild radius.)

Now we discuss the values of the model parameters. As stated in § 1, the exact value of α is uncertain, and we adopt $\alpha = 0.3$, which appears to be the highest possible value. This choice allows us to show the highest values of L possible in the ADAF model, and it shows that even then that model cannot explain the luminous hard states of BHXBs. We set the magnetic parameter β, defined as the ratio of the gas pressure to the sum of the gas and magnetic pressures, to be $\beta = 0.9$ (from MHD numerical simulations; e.g., Hawley & Krolik 2001), and the fraction of the viscous dissipation directly heating electrons is set at $\delta = 0.5$ (from modeling of the supermassive black hole in our Galactic center; Yuan et al. 2003). The parameters α, β, and δ are not free hereafter, although we realize that their values carry large uncertainties. The outer radius of the cold disk is set equal to the tidal radius, which is ~87% of the Roche lobe radius (Papaloizou & Pringle 1977). The Roche lobe radius is 55%–59% of the separation (Eggleton 1983) for the estimated mass ratio of the black hole to the companion of 6.7–11, while the separation itself is $\simeq 9 \times 10^{11}$ cm (Orosz et al. 2002). This implies an outer radius of $\simeq 5 \times 10^{11}$ cm, equivalent to $\simeq 1.5 \times 10^5 (10\ M_\odot/M) r_{\rm S}$. We set the black hole mass to $M = 10.5\ M_\odot$ and the distance to $D = 5.3$ kpc (Orosz et al. 2002).[7]

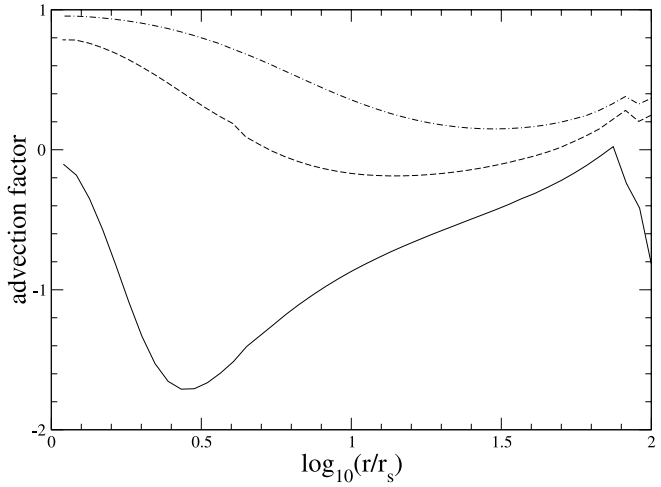

FIG. 2.—Profile of the advection factor (defined in eq. [2]) for the three models shown in Fig. 1. The model denoted by the dot-dashed curve is an ADAF, since its advection factor is always positive, while the other two models are LHAFs, since their advection factors are negative in some regions. The irregular behavior near $100 r_{\rm S}$ is an effect of the boundary condition.

Another important parameter is the transition radius, $r_{\rm tr}$. As shown in Yuan et al. (2005), its value is best constrained by the thin disk emission close to $r_{\rm tr}$, which is in the EUV/soft X-ray band. However, we have no data for that band and hereafter assume $r_{\rm tr} = 100 r_{\rm S}$. As stated above, most of the seed photons for Comptonization at this value of $r_{\rm tr}$ are synchrotron photons from the hot accretion flow. Our satisfactory fits to the data (Fig. 1, *magenta*, *green*, *and red*) indicate that our solution is viable, although it may be not unique.

On the other hand, it is possible that when the hard state approaches the very high state, the soft photons from the thin disk or clumps in the hot accretion flow become dominant (see also Wardziński & Zdziarski 2000). As shown in Yuan et al. (2007), the X-ray slope of (at least some) black hole binaries is correlated with the luminosity, L, and the sign of the correlation changes when the luminosity of the hard state increases above a certain value. Below this luminosity the X-ray spectrum hardens with increasing L, and above it, it softens. The boundary in our case approximately corresponds to the MJD 51,646 spectrum in Figure 1 (*red*), though in our case, with a limited range of L, the X-ray spectra below it maintain an approximately constant slope. The change in the sign of the correlation may be due to a change in the dominant source of the seed photons.

2.3. *Modeling Results*

Figure 1 shows our X-ray spectral fits to the lower three hard states. (We discuss the brightest hard state separately.) From bottom to top, they are shown by the dot-dashed, dashed, and solid curves and have ($\dot{M}_0/\dot{M}_{\rm E}$, s_0) equal to (1.0, 0.55), (1.1, 0.3), and (1.3, 0.3), respectively. The advection factor, f, and the electron temperature, T_e, of these models are shown as a function of r in Figures 2 and 3, respectively.

[7] Jonker & Nelemans (2004) argued that the distance to XTE J1550−564 might have been underestimated by as much as a factor of 3 due to an overestimation of the interstellar extinction. However, if this were true, the highest 1–20 keV luminosity of the 1998 outburst would be $\sim 10 L_{\rm E}$, which seems highly unlikely.

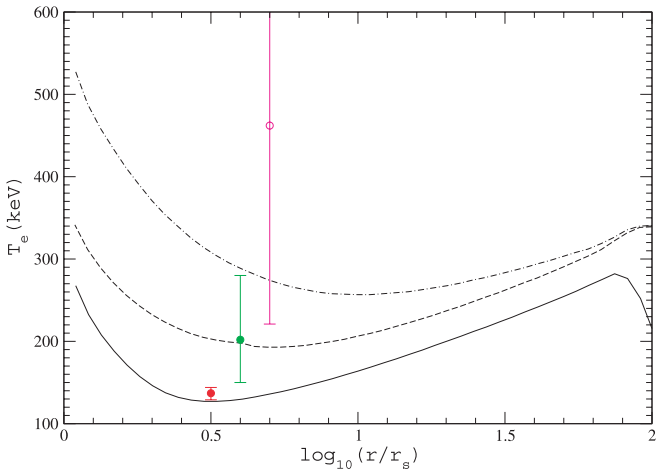

FIG. 3.—Profiles of the electron temperature for the three models shown in Fig. 1. With an increase in accretion rate, the electron temperature decreases, consistent with the observed anticorrelation between the *e*-folding energy E_f and the luminosity seen in Fig. 1. The three different-colored circles show the E_f for the corresponding three X-ray spectra shown in Fig. 1. Their abscissa is arbitrary. The magenta circle denotes the *e*-folding energy poorly constrained by the data. Since E_f is proportional to the electron temperature, these results show that the hot accretion flow models (ADAF and LHAF) can quantitatively predict the correct electron temperature.

One can see in Figure 1 that the three models fit the X-ray spectra relatively well, including both the spectral slope and the cutoff energy. E97 did not take into account outflows and predicted that the X-ray spectra from hot accretion flows should harden with increasing accretion rate. The X-ray spectrum at MJD 51,646 (*red*) is harder than that at MJD 51,687 (*green*), consistent with that prediction. However, the slope of the spectrum at MJD 51,687 is identical to that at MJD 51,696 (*magenta*), which is different from the prediction of E97. Our calculations show that the inclusion of the outflow in our model can mostly resolve this discrepancy. From equations (1)–(2) and Figure 2, we see that there is no outflow for the model shown by the solid curve, since its advection factor is $f < 0$. For the dashed-line model, f is very small: $f \approx 0$, so the outflow is also weak. Since the accretion rate represented by the solid curve is larger than that of the dashed curve, the former spectrum is harder. On the other hand, for the dot-dashed curve, $s_0 = 0.55$ and $f \sim 1$, the outflow is strong.

Thus, the presence of an outflow will make the emitted spectrum harder compared with that with no outflow at the same $\dot{M}_0$. For comparison, we also show in Figure 1 the spectrum produced by a model without outflow (at $\dot{M}_0 = 0.5\dot{M}_{\rm E}$, to reproduce the X-ray flux level; *double-dot–dashed curve*). One can clearly see that its spectrum is softer than that of the dot-dashed curve (including the outflow). The physical reason for this is as follows: The emitted X-ray spectrum is the sum of the local Comptonization spectra at each radius, and the slope of that spectrum is determined by the Compton *y*-parameter, with a larger *y* corresponding to a harder spectrum (e.g., Beloborodov 1999). At small radii *y* is relatively small, so the corresponding spectrum is soft. When a strong outflow exists, the accretion rate decreases with decreasing radius, and thus the contribution of the innermost region becomes smaller. Therefore, the total spectrum will become harder. We note that this effect is not universal; it holds only for a certain range of the accretion rate.

We note that the spectra produced by all three models are somewhat too soft in comparison with the X-ray data. Slightly increasing $\dot{M}_0$ can make the spectrum harder, thus improving the fits. However, the corresponding luminosities will be higher than the observed values. Given the uncertainty in the distance of XTE J1550−564, it is possible that the distance is slightly larger than $D = 5.3$ kpc. Another solution would be to use a larger β, which would reduce the magnetic field and thus the synchrotron emission. As the latter provides seed photons for Comptonization, this will lead to a hardening of the spectra.

Our models also fit satisfactorily the *e*-folding energies E_f. As noted in § 2.1, E_f is anticorrelated with the X-ray luminosity. Such an anticorrelation appears to be common in the hard states. It takes place, for example, in GRO J0422+32 (Grove et al. 1998) and GX 339−4 (Wardziński et al. 2002). In thermal Comptonization models, E_f is close to the electron temperature T_e. Such an anticorrelation between T_e and L (or $\dot{M}$) is expected in the hot accretion flow models, both ADAF and LHAF, as illustrated here in Figure 3 (see also Fig. 3*b* of E97), which shows the T_e-profiles of the three models shown in Figure 1, together with the values of E_f of the observed X-ray spectra. Note that the value of E_f for the lowest considered state is not precisely determined. Since the emitted X-ray spectra are integrated over the radii, the E_f here only measures an average T_e. Still, the agreement shown is excellent, indicating that the hot accretion flow model is able to quantitatively predict the correct E_f. We emphasize that this result is quite robust, independent of the model parameters. It provides strong support for this model of the hard state.

Let us now discuss the dynamics of the accretion flow. We first need to illustrate the physics of the LHAF. The energy equation for ions in hot accretion flows reads $q_{\rm adv} \equiv q_{\rm int} - q_{\rm comp} = q_{\rm vis} - q_{\rm ie}$. The subscripts denote energy advection, the gradient of the internal energy of ions, compression work, viscous heating, and Coulomb collision cooling, respectively. The critical accretion rate of an ADAF, $\dot{M}_{\rm ADAF}$, is determined by $q_{\rm vis} = q_{\rm ie}$ (Narayan et al. 1998). Below $\dot{M}_{\rm ADAF}$, $q_{\rm vis} > q_{\rm ie}$, and therefore we have $q_{\rm int} = q_{\rm comp} + q_{\rm vis} - q_{\rm ie} > 0$. The positive sign of $q_{\rm int}$ means that the flow can remain hot if it starts out hot (because $q_{\rm int} \propto v\, dT/dr$, and $v < 0$). This is why a hot ADAF solution can exist. Above $\dot{M}_{\rm ADAF}$ up to another (higher) critical accretion rate determined by $q_{\rm vis} + q_{\rm comp} = q_{\rm ie}$, the value of $q_{\rm int}$ ($=q_{\rm comp} + q_{\rm vis} - q_{\rm ie}$) is still positive. Thus, a new hot accretion solution, that is, LHAF, exists between $\dot{M}_{\rm ADAF}$ and this new rate (Y01). For an ADAF, $q_{\rm adv} > 0$, so advection plays a cooling role, while in an LHAF, $q_{\rm adv} < 0$, so advection plays a heating role. In this case, the radiative cooling is balanced by the sum of advective and viscous heating.

In Figure 2, we see that the advection factor for the dot-dashed curve is greater than 0, and thus it represents an ADAF. The bolometric luminosity of this model is $L \sim 0.008 L_{\rm E}$. The advection factor for the dashed curve is negative in some regions, and thus it is marginally an LHAF, with $L \sim 0.03 L_{\rm E}$. This result is roughly consistent with those of E97, who found the highest accretion rate of ADAFs to be $\dot{M}_{\rm ADAF} \approx 13\alpha^2 \dot{M}_{\rm E} \approx \dot{M}_{\rm E}$, and the corresponding highest L is $\simeq 0.4\alpha^2 L_{\rm E} \approx (0.03$–$0.04)\, L_{\rm E}$ for $\alpha = 0.3$. Thus, for spectra such as that from MJD 51,687, whose L is $\sim 0.03 L_{\rm E}$, an ADAF marginally fails to work. For the spectrum at MJD 51,646, the luminosity is still higher, $\sim 0.06 L_{\rm E}$. In this case, the flow is an LHAF in the entire range (Fig. 2, *solid curve*).

However, even an LHAF cannot explain the spectrum at MJD 51,658 (Fig. 1, *blue*). This is because the required L is above the maximum LHAF accretion rate, $\dot{M}_{\rm LHAF}$, roughly determined by $q_{\rm vis} + q_{\rm comp} = q_{\rm ie}$. Because $q_{\rm comp}$ does not depend on α, the value of $\dot{M}_{\rm LHAF}$ depends only weakly on α, unlike $\dot{M}_{\rm ADAF}$. In addition to α, other model parameters such as β and δ and the outer boundary condition also affect its value. Y01 found that $\dot{M}_{\rm LHAF}/\dot{M}_{\rm E} \simeq 5$ and 3 for $\alpha = 0.3$ and 0.1, respectively. For the

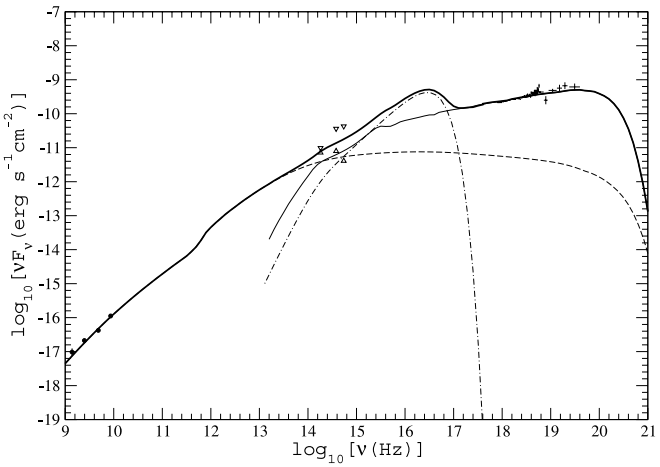

FIG. 4.— Accretion/jet model for XTE J1550−564 at MJD 51,696. The dashed, thin solid, and dot-dashed curves show the emission from the jet, the LHAF, and the truncated thin disk, respectively. The jet emission contributes significantly at the *H*, *I*, and *V* bands. On the other hand, the jet contribution is negligible in the X-ray band. This explains why we see secondary peaks at the *H*, *I*, and *V* bands with no corresponding peak at the X-ray band. (See § 3 for details.)

parameters adopted here, $\dot{M}_{\rm LHAF}$ is slightly larger than $1.3\dot{M}_{\rm E}$,[8] which corresponds to $L \lesssim 0.08L_{\rm E}$. This is not high enough to explain the X-ray spectrum at MJD 51,658. When $\dot{M}_0 \gtrsim \dot{M}_{\rm LHAF}$, the innermost region of the LHAF will collapse and form a cold annulus (Y01). Calculations of the emitted spectrum in this case are complicated; here we hypothesize that this effect may be responsible for the very high state.

Phenomenologically, the X-ray spectrum at MJD 51,658 appears to be intermediate between the hard-state spectra and the very high state spectrum (Fig. 1, *black points*). The approximate agreement between the observed highest luminosity of the proper hard state and the highest LHAF luminosity strongly supports the LHAF models for the luminous hard state of BHXBs.

Figure 1 shows that the IR/optical fluxes are underpredicted by the hot-flow models. This implies that some other components such as a jet and the thin disk also contribute. We consider the role of the jet in § 3. Here we show the emission from an irradiated truncated thin disk with $\dot{M} = 1.3\dot{M}_{\rm E}$ and $r_{\rm tr} = 100r_{\rm S}$. We see that this improves the agreement of the model with the data in the optical band, but most of the IR data are still not explained.

3. ROLE OF THE JET

We note here two interesting results in the IR/optical and X-ray light curves for the 2000 outburst reported by J01. The first is that the outburst in the IR/optical started some days before that in X-rays (seen by the *RXTE* All-Sky Monitor). Here we focus on another interesting result from J01. After the primary peak of the outburst, the *H*, *I*, and *V* and X-ray fluxes declined, and the transition from the very high state back to the hard state occurred around MJD 51,680. After the transition, the X-ray flux continued to decline, while the *H*, *I*, and *V* fluxes began to rise and reached secondary maxima at MJD 51,699–51,705. J01 also found that the secondary maximum is most prominent in the *H* band.

The IR/optical and X-ray spectra at MJD 51,696 are shown in Figure 4, which also shows the contemporaneous radio measurements at MJD 51,697 (Corbel et al. 2001) by the Australia Telescope Compact Array, at four frequencies from 1384 to 8640 MHz. The detected spectrum is slightly inverted, with a spectral index of $\alpha_R = 0.37 \pm 0.10$ (where the energy flux is $F_\nu \propto \nu^{\alpha_R}$). Since the radio regime is much less variable than the X-rays, we assume that the radio spectra at MJD 51,696 and 51,697 were the same.

Based on Figure 4, we can rule out the standard thin disk as the origin of the secondary peaks in *H*, *I*, and *V*. The flux produced by the thin disk in the *H* band depends mainly on the values of the outer radius of the thin disk, $r_{\rm out}$, and $\dot{M}$. The dot-dashed curve in Figure 4 shows the emitted spectrum from an irradiated thin disk with $\dot{M}_0 = 1.0\dot{M}_{\rm E}$ and $r_{\rm out} = 1.5 \times 10^5 r_{\rm S}$. One can see that the emission from the disk (in the Rayleigh-Jeans regime) is substantially below the observed *H*-band flux. We note that only for $\dot{M} \sim 40\dot{M}_{\rm E}$, which appears highly unlikely, would the observed and predicted *H* fluxes become equal.

Jet formation is usually observed when the source enters the hard state (Fender 2001, 2006). Prompted by this, J01 proposed that the secondary peaks are due to the emission from the jet formed at the time of the very high–hard state transition around MJD 51,680. Our detailed calculations support this conjecture. We model the MJD 51,696 spectrum (Fig. 4) taking into account the contributions from the hot flow, the truncated disk, and the jet. We use the internal shock scenario (widely adopted in the study of gamma-ray burst afterglows) to calculate the jet emission (see Yuan et al. 2005 for details). Briefly, internal shocks within the jet occur as a consequence of collisions of shells with different velocities. The shocks accelerate a fraction of the electrons into a nonthermal, power-law energy distribution. The steady state electron energy distribution is then self-consistently determined by taking into account the radiative cooling. We parameterize the model with two parameters, ϵ_e and ϵ_B, giving the fraction of the shock energy going into the accelerated electrons and the (amplified) magnetic field, respectively. We then calculate the nonthermal synchrotron emission.

The modeled jet and total spectra are shown by the dashed and solid curves, respectively, in Figure 4. One can see that this model fits the data from the radio to the X-rays very well. The jet parameters are $\epsilon_e = 0.06$ and $\epsilon_B = 0.02$, its opening angle is $\theta = 0.1$, the bulk Lorentz factor $\Gamma_{\rm jet} = 1.2$, and the spectral index at which the electrons are accelerated is $p = 2.23$. The values of the parameters are the same as those used in Yuan et al. (2005) to model the outburst hard state of XTE J1118+480. The mass flow through the jet is $\dot{M}_{\rm jet} = 3.3 \times 10^{-3}\dot{M}_{\rm E}$. This is ~0.6% of the accretion rate at the inner flow, equal to $0.54\dot{M}_{\rm E}$ at $5r_{\rm S}$. This is very similar to the corresponding value of 0.5% in XTE J1118+480.

Based on the above fitting, we now explain the secondary peaks in *H*, *I*, and *V* as follows: The jet began to form at the very high–to–hard state transition, at MJD 51,680. Initially $\dot{M}_{\rm jet}$ was very small, and therefore the contribution of the jet emission to the *H* flux was negligible. But then the accretion $\dot{M}$ continued to decrease and the accretion luminosity declined. On the other hand, the jet grew, with $\dot{M}_{\rm jet}$ increasing, so the relative jet contribution to the *H*, *I*, and *V* bands continued to increase. The increase of $\dot{M}_{\rm jet}$ lasted for ~20 days and reached its maximum at MJD 51,699–51,705, which corresponds to the secondary peaks in the *H*, *I*, and *V* light curves. After that time, $\dot{M}_{\rm jet}$ decreased together with $\dot{M}$. Our fitting results at MJD 51,696 shown in Figure 4 are for the time very close to that of the secondary peaks in *H*, *I*, and *V*.

Figure 1 of J01 shows that the *H*-band fluxes at MJD 51,680 and 51,696 differ by 1 mag. We note that the modeled ADAF and the thin disk fluxes could have changed only very little between

[8] As a comparison, the critical rate of the ADAF for the parameters adopted in the present paper is $\dot{M}_{\rm ADAF} \simeq 1.1\dot{M}_{\rm E}$. The ratio $\dot{M}_{\rm LHAF}/\dot{M}_{\rm ADAF}$ is smaller than that obtained in Y01. This is due to the different parameters assumed, α, β, and δ, as well as to the inclusion of outflows in the ADAF but not in the LHAF (where they are suppressed).

those two days (see Fig. 1). On the other hand, from Figure 4 we see that the *H*-band flux increases as a result of the appearance of the jet emission at MJD 51,696 by about 1 mag, completely consistent with the observational results from J01. We also see in Figure 4 that while the νF_ν spectrum from the jet is almost flat in the *H*, *I*, and *V* bands, the spectrum of the accretion flow (the thin disk and ADAF) rises with increasing frequency. This explains why the secondary peak is most prominent in the *H* band (J01), that is, at the lowest energy.

Another important observational result is the absence of the corresponding secondary peak in the X-ray light curve. This requires that whatever emission the jet produces in X-rays has to be negligible compared with that from the hot accretion flow. Our theoretical modeling is consistent with that result. As shown in Figure 4, the contribution of the jet emission in the X-ray band is much weaker than that of the accretion flow. We thus conclude that the absence of the secondary maximum in the X-ray light curve provides strong evidence that the jet emission (synchrotron plus Compton) is not important in the X-ray band in the hard state.

4. SUMMARY AND DISCUSSION

We have investigated the hard states of XTE J1550−564 during its 2000 outburst. We modeled the X-ray spectra with accretion flow models (§ 2). Our model consists of an inner hot flow within a transition radius and an outer thin disk, as in E97. Differently from E97, we have taken into account two new developments in the hot accretion flow models. One is the inclusion of outflow, and the other is the extension of the ADAF model to higher accretion rates using the LHAF model (Y01). Our model fits well the lower three of the four characteristic hard-state spectra (see Fig. 1). The two extensions of the model are necessary for the obtained good fits. First, the inclusion of the outflow allows us to fit the X-ray spectral slopes. Without outflow, the emitted spectrum hardens with increasing accretion rate (E97), which disagrees with the observations, where the slopes of the two lowest data sets are almost identical despite their different luminosities. To resolve this discrepancy, the outflow becomes weaker with increasing accretion rate. This is physically motivated, as the radiative energy loss is smaller at lower accretion rates and thus the Bernoulli parameter is larger.

The extension of hot accretion flow models from ADAFs to LHAFs enables us to model the luminous hard states with luminosities up to $\sim 0.08 L_{\rm E}$ (while the ADAF is limited to $\lesssim 0.03 L_{\rm E}$). The LHAF fits the spectral slope and the cutoff energy of those states, as shown in Figure 1, confirming the prediction of Yuan & Zdziarski (2004).

The value of the highest possible luminosity of the LHAF model, $L_{\rm LHAF}$, depends on α and other model parameters and the outer boundary condition (see Y01). For our assumed parameters we find $L_{\rm LHAF} \simeq 0.08 L_{\rm E}$, somewhat lower than the L of the most luminous hard state considered here (Fig. 1, *blue symbols*). However, we can see that this state appears intermediate between the hard and the very high states, and perhaps some processes responsible for the very high state are already of importance here. Thus, the overall agreement between the maximum observed L and the prediction of the LHAF model provides strong support for it as a model of the X-ray emission of the hard states of BHXBs.

The highest L of the hard state varies among various sources, as well as different outbursts of a given source. As discussed in § 1, the maximum hard-state L of XTE J1550−564 and GX 339−4 varies in the ∼10%–30% range. On the other hand, the corresponding value in Cyg X-1 is only $\sim 0.01-0.02 L_{\rm E}[d/(2\ {\rm kpc})]^2 (10\, M_\odot/M)$ (e.g., Zdziarski et al. 2002). We now discuss possible reasons for this variability.

First, $L_{\rm LHAF}$ is a function of the model parameters, for example, α, and parameter variations among different sources will contribute to its dispersion. However, numerical simulations of accretion flows indicate that $\alpha < 0.3$ (e.g., Hawley & Krolik 2001). Thus, this effect can explain a low value of the maximum L but not values $\gtrsim 0.10 L_{\rm E}$. Still, we can obtain $\sim 0.15 L_{\rm E}$ by adjusting the outer boundary condition (determined by the physics of the transition region between the hot and cool accretion flows, which is complex and currently unclear).

An efficient way of increasing the maximum hard-state L can be allowing the angular momentum of the black hole to be nonzero. In the present calculations, we have assumed a Schwarzschild black hole. If the black hole is rapidly rotating, substantially more gravitational energy will be released because of the deeper potential well (e.g., Gammie & Popham 1998; Popham & Gammie 1998). Shafee et al. (2006) indeed have found that a number of BHXBs appear to have spin parameters of ∼0.6–0.8.

Yet another effect that could increase $L_{\rm LHAF}$ is a magnetic coupling between the rotating black hole and the accretion flow. If the black hole rotates faster than the disk, energy and angular momentum will be extracted from the black hole and transferred to the disk by the magnetic field (Li 2000, 2002; Wang et al. 2003). However, we are not able to estimate quantitatively the importance of this effect here, because the existing studies have only considered the standard thin disk rather than a hot flow.[9]

As we pointed out above, the most luminous hard states border the very high state. The nature of the latter remains an open question. Numerical calculations by Y01 (see also Begelman et al. 1987) indicate that above $\dot{M}_{\rm LHAF}$, the hot accretion flow will collapse within a certain radius and form a cold annulus (see Liu et al. [2006] for a similar result in the context of their evaporation model). The inner cold annulus will emit blackbody radiation, which may explain the thermal component of the very high state. At the collapse region, strong magnetic reconnection events should occur due to the overflow of the magnetic field (Begelman et al. 1987; Y01). This is likely to accelerate some electrons into a power-law distribution. Compton scattering of the soft photons from the inner annulus by both the thermal and power-law electrons may then be responsible for the X-ray emission of the very high state. We note that Gierliński & Done (2003) have found that the shape of the soft γ-ray spectrum of XTE J1550−564 in the very high state indeed requires the presence of both thermal and nonthermal (power-law–like) electrons.

A possible problem with the above scenario is that the hot accretion flow is strongly thermally unstable at the collapse region (Yuan 2003). As a result of the instability, the accretion flow may form a two-phase flow structure, with cold clumps surrounded by the hot phase (Guilbert & Rees 1988; Celotti et al. 1992; Kuncic et al. 1997; Krolik 1998; Beloborodov 1999; Yuan 2003; Merloni et al. 2006). The radiation from the cold clumps can then explain the thermal component of the very high state, whereas Comptonization of the soft photons by the high-energy electrons in the hot phase may be responsible for the power-law tail. Thus, this represents an alternative scenario for the very high state. (However, a hybrid electron distribution in the hot phase is required, as stated above; see Gierliński & Done 2003.) We speculate that even

[9] Recently, attention has been paid to the effect of the presence of magnetic stresses near and inside the last stable circular orbit on the radiative efficiency of the standard thin disk (e.g., Agol & Krolik 2000; Beckwith et al. 2006). This effect does not apply to the hot accretion flow, since the no-torque boundary condition is not adopted in the global solution of hot accretion flow.

some luminous hard-state flows with $\dot{M} \lesssim \dot{M}_{\rm LHAF}$ may also contain such a two-phase configuration. The formation of the cold clumps in this case could be due to the strong instability in the transition region between the hot accretion flow and the standard thin disk (Kato 1999, 2000). This scenario is promising in explaining the observed power spectra of the rapid aperiodic variability of X-ray emission of BHXBs (Böttcher & Liang 1999). It also may explain the claimed relativistic iron K emission line profiles in BHXBs (e.g., Miller et al. 2006). We plan to investigate these issues in future work.

We have also investigated the nature of the secondary peaks in the *H*, *I*, and *V* light curves of XTE J1550−564 (J01). They began to emerge after the transition from the very high state back to the hard state and reached a maximum ∼20 days later. However, there have been no corresponding peaks in the X-ray light curve. Based on detailed modeling to the multiwaveband spectrum from the radio to X-rays, we conclude that the secondary peaks are due to the emission from the jet formed during the state transition. The mass-loss rate in the jet kept increasing for ∼20 days after its birth and then decreased. The secondary peaks were then due to the corresponding maximum of the relative contribution of the jet (*H*, *I*, *V*) emission with respect to the accretion emission. The absence of a corresponding peak in the X-rays strongly indicates that the jet emission (either synchrotron or Compton) is negligible in the X-ray band in the hard state. This differs from the scenarios in which the jet dominates in X-rays (e.g., Markoff et al. 2005). In principle, it is possible that a drop in the X-ray flux from the disk is exactly compensated by a rise in the X-ray flux from the jet, with the total flux changing smoothly. As this scenario requires fine-tuning, we consider it to be highly unlikely.

We also point out that Xue et al. (2006) present another argument against jet dominance in X-rays in the hard state. By modeling the spectrum of the jet blob, they obtained the parameters of the electron energy distribution. Assuming the electron energy distribution is the same for all blobs in the jet, they model the overall radio spectrum of the source and extrapolate their fit to higher energies. They find that the synchrotron emission from the jet contributes negligibly to the observed X-ray emission.

We thank John Tomsick and the referee, Chris Done, for valuable comments. This work was supported in part by the National Natural Science Foundation of China (grant 10543003), the Shanghai Pujiang Talent Program, and the Hundred Talent Program of China (F. Y.), and by grants 1P03D01827, 1P03D01128, and 4T12E04727 from the Polish State Committee for Scientific Research (A. A. Z.).

REFERENCES

Abramowicz, M. A., Chen, X., Kato, S., Lasota, J.-P., & Regev, O. 1995, ApJ, 438, L37
Agol, E., & Krolik, J. H. 2000, ApJ, 528, 161
Beckwith, K., Hawley, J. F., & Krolik, J. H. 2006, ApJ, submitted (astro-ph/0605295)
Begelman, M. C., Sikora, M., & Rees, M. J. 1987, ApJ, 313, 689
Beloborodov, A. M. 1999, in ASP Conf. Ser. 161, High Energy Processes in Accreting Black Holes, ed. J. Poutanen & R. Svensson (San Francisco: ASP), 295
Blandford, R. D., & Begelman, M. C. 1999, MNRAS, 303, L1
Böttcher, M., & Liang, E. P. 1999, ApJ, 511, L37
Celotti, A., Fabian, A. C., & Rees, M. J. 1992, MNRAS, 255, 419
Chaty, S., Haswell, C. A., Malzac, J., Hynes, R. I., Shrader, C. R., & Cui, W. 2003, MNRAS, 346, 689
Coppi, P. S., & Blandford, R. D. 1990, MNRAS, 245, 453
Corbel, S., et al. 2001, ApJ, 554, 43
Done, C., & Gierliński, M. 2003, MNRAS, 342, 1041
Eggleton, P. P. 1983, ApJ, 268, 368
Esin, A. A., McClintock, J. E., Drake, J. J., Garcia, M. R., Haswell, C. A., Hynes, R. I., & Muno, M. P. 2001, ApJ, 555, 483
Esin, A. A., McClintock, J. E., & Narayan, R. 1997, ApJ, 489, 865 (erratum 500, 523 [1998]) (E97)
Fender, R. 2006, in Compact Stellar X-Ray Sources, ed. W. H. G. Lewin & M. van der Klis (Cambridge: Cambridge Univ. Press), 381
Fender, R. P. 2001, MNRAS, 322, 31
Frontera, F., Amati, L., Zdziarski, A. A., Belloni, T., Del Sordo, S., Masetti, N., Orlandini, M., & Palazzi, E. 2003, ApJ, 592, 1110
Frontera, F., et al. 2001, ApJ, 561, 1006
Galeev, A. A., Rosner, R., & Vaiana, G. S. 1979, ApJ, 229, 318
Gammie, C. F., & Popham, R. 1998, ApJ, 498, 313
Gierliński, M., & Done, C. 2003, MNRAS, 342, 1083
Grove, J. E., Johnson, W. N., Kroeger, R. A., McNaron-Brown, K., Skibo, J. G., & Phlips, B. F. 1998, ApJ, 500, 899
Guilbert, P. W., & Rees, M. J. 1988, MNRAS, 233, 475
Hawley, J. F., & Balbus, S. A. 2002, ApJ, 573, 738
Hawley, J. F., & Krolik, J. H. 2001, ApJ, 548, 348
Hirose, S., Krolik, J. H., & Stone, J. M. 2006, ApJ, 640, 901
Hynes, R. I., Mauche, C. W., Haswell, C. A., Shrader, C. R., Cui, W., & Chaty, S. 2000, ApJ, 539, L37
Igumenshchev, I. V., Narayan, R., & Abramowicz, M. A. 2003, ApJ, 592, 1042
Jain, R. K., Bailyn, C. D., Orosz, J. A., McClintock, J. E., & Remillard, R. A. 2001, ApJ, 554, L181 (J01)
Jonker, P. G., & Nelemans, G. 2004, MNRAS, 354, 355
Kato, S. 1999, PASJ, 51, 71
———. 2000, PASJ, 52, 1125
Krolik, J. H. 1998, ApJ, 498, L13
Kuncic, Z., Celotti, A., & Rees, M. J. 1997, MNRAS, 284, 717
Li, L.-X. 2000, ApJ, 533, L115
———. 2002, ApJ, 567, 463
Liang, E. P. T., & Price, R. H. 1977, ApJ, 218, 247
Liu, B. F., Meyer, F., & Meyer-Hofmeister, E. 2006, A&A, 454, L9
Malzac, J., Merloni, A., & Fabian, A. C. 2004, MNRAS, 351, 253
Manmoto, T., Mineshige, S., & Kusunose, M. 1997, ApJ, 489, 791
Markoff, S., Nowak, M. A., & Wilms, J. 2005, ApJ, 635, 1203
McClintock, J. E., & Remillard, R. A. 2006, in Compact Stellar X-Ray Sources, ed. W. H. G. Lewin & M. van der Klis (Cambridge: Cambridge Univ. Press), 157
McClintock, J. E., et al. 2001, ApJ, 555, 477
Merloni, A., Malzac, J., Fabian, A. C., & Ross, R. R. 2006, MNRAS, 370, 1699
Miller, J. M., Homan, J., Steeghs, D., Rupen, M., Hunstead, R. W., Wijnands, R., Charles, P. A., & Fabian, A. C. 2006, ApJ, 653, 525
Narayan, R. 1996, ApJ, 462, 136
Narayan, R., Igumenshchev, I. V., & Abramowicz, M. A. 2000, ApJ, 539, 798
Narayan, R., Mahadevan, R., & Quataert, E. 1998, in Theory of Black Hole Accretion Discs, ed. M. A. Abramowicz, G. Björnsson, & J. E. Pringle (Cambridge: Cambridge Univ. Press), 148
Narayan, R., McClintock, J. E., & Yi, I. 1996, ApJ, 457, 821
Narayan, R., & Yi, I. 1994, ApJ, 428, L13
———. 1995, ApJ, 452, 710
Orosz, J. A., et al. 2002, ApJ, 568, 845
Papaloizou, J., & Pringle, J. E. 1977, MNRAS, 181, 441
Popham, R., & Gammie, C. F. 1998, ApJ, 504, 419
Quataert, E., & Gruzinov, A. 2000, ApJ, 539, 809
Rees, M. J., Phinney, E. S., Begelman, M. C., & Blandford, R. D. 1982, Nature, 295, 17
Rodriguez, J., Corbel, S., & Tomsick, J. A. 2003, ApJ, 595, 1032
Sánchez-Fernández, C., et al. 1999, A&A, 348, L9
Shafee, R., McClintock, J. E., Narayan, R., Davis, S. W., Li, L.-X., & Remillard, R. A. 2006, ApJ, 636, L113
Shapiro, S. L., Lightman, A. P., & Eardley, D. M. 1976, ApJ, 204, 187
Sobczak, G. J., McClintock, J. E., Remillard, R. A., Cui, W., Levine, A. M., Morgan, E. H., Orosz, J. A., & Bailyn, C. D. 2000, ApJ, 544, 993
Stone, J. M., Pringle, J. E., & Begelman, M. C. 1999, MNRAS, 310, 1002
Tomsick, J. A., Corbel, S., & Kaaret, P. 2001, ApJ, 563, 229
Wang, D.-X., Ma, R.-Y., Lei, W.-H., & Yao, G.-Z. 2003, ApJ, 595, 109
Wardziński, G., & Zdziarski, A. A. 2000, MNRAS, 314, 183
Wardziński, G., Zdziarski, A. A., Gierliński, M., Grove, J. E., Jahoda, K., & Johnson, W. N. 2002, MNRAS, 337, 829
Xue, Y., Wu, X.-B., & Cui, W. 2006, A&A, submitted (astro-ph/0606194)

Yuan, F. 2001, MNRAS, 324, 119 (Y01)
———. 2003, ApJ, 594, L99
Yuan, F., Cui, W., & Narayan, R. 2005, ApJ, 620, 905
Yuan, F., Quataert, E., & Narayan, R. 2003, ApJ, 598, 301
Yuan, F., Taam, R. E., Misra, R., Wu, X.-B., & Xue, Y. 2007, ApJ, 658, 282
Yuan, F., & Zdziarski, A. A. 2004, MNRAS, 354, 953
Zdziarski, A. A. 2000, in IAU Symp. 195, Highly Energetic Physical Processes and Mechanisms for Emission from Astrophysical Plasmas, ed. P. C. H. Martens, S. Tsuruta, & M. A. Weber (San Francisco: ASP), 153
Zdziarski, A. A., & Gierliński, M. 2004, Prog. Theor. Phys. Suppl., No. 155, 99
Zdziarski, A. A., Gierliński, M., Mikołajewska, J., Wardziński, G., Smith, D. M., Harmon, B. A., & Kitamoto, S. 2004, MNRAS, 351, 791
Zdziarski, A. A., Poutanen, J., Paciesas, W. S., & Wen, L. 2002, ApJ, 578, 357